JOURNAL OF GEOPHYSICAL RESEARCH, VOL. 113, E06S21, doi:10.1029/2007JE003022, 2008

Depth selective Mössbauer spectroscopy: Analysis and simulation of 6.4 keV and 14.4 keV spectra obtained from rocks at Gusev Crater, Mars, and layered laboratory samples

I. Fleischer,[1] G. Klingelhöfer,[1] C. Schröder,[2] R. V. Morris,[2] M. Hahn,[1] D. Rodionov,[1,3] R. Gellert,[4] and P. A. de Souza[5,6]

Received 14 October 2007; revised 7 March 2008; accepted 28 April 2008; published 26 June 2008.

[1] The miniaturized Mössbauer spectrometer (MIMOS) II Mössbauer spectrometers on the Mars Exploration Rovers (MER) simultaneously obtained 6.4 keV and 14.4 keV Mössbauer spectra from rock and soil targets. Because photons with lower energy have a shallower penetration depth, 6.4 keV spectra contain more mineralogical information about the near-surface region of a sample than do 14.4 keV spectra. The influence of surface layers of varying composition and thickness on Mössbauer spectra was investigated by Monte Carlo simulation and by measurement using a copy of the MER MIMOS II instrument and samples with one or two layers of known thicknesses. Thin sections of minerals or metallic Fe foil on top of a thick mineral sample were used to produce samples with thin layers of known thickness on a thick substrate. Monte Carlo simulation of MER spectra obtained on the rock Mazatzal, which displays a coating on a basaltic substrate, and other Adirondack Class rocks results in a calculated thickness of 10 μm for the Mazatzal surface layer. The 6.4 keV spectra obtained on Adirondack Class rocks, on laboratory samples, and in Monte Carlo calculations show an apparent olivine enrichment which is not related to any observable surface layer.

Citation: Fleischer, I., G. Klingelhöfer, C. Schröder, R. V. Morris, M. Hahn, D. Rodionov, R. Gellert, and P. A. de Souza (2008), Depth selective Mössbauer spectroscopy: Analysis and simulation of 6.4 keV and 14.4 keV spectra obtained from rocks at Gusev Crater, Mars, and layered laboratory samples, *J. Geophys. Res.*, *113*, E06S21, doi:10.1029/2007JE003022.

1. Introduction

[2] The Mars Exploration Rovers (MER) Spirit and Opportunity have investigated the Martian surface since their landing in January 2004. Spirit landed on the plains of the 160 km diameter Gusev crater, and Opportunity landed on the plains of Meridiani Planum. The primary objective of their mission is to explore two sites on the Martian surface where water may once have been present [*Squyres et al.*, 2004]. Both rovers carry mast-mounted remote sensing instruments and in situ instruments mounted on a 5 degree-of-freedom instrument deployment device (IDD). The remote sensing instruments are a multispectral Panoramic camera (Pancam) and a Miniature Thermal Emission Spectrometer (Mini-TES). The in situ instruments are an Alpha Particle X-ray Spectrometer (APXS), a Microscopic Imager (MI), a Rock Abrasion Tool (RAT), and a miniaturized Mössbauer spectrometer (MB). The Mössbauer instruments can simultaneously collect 6.4 keV X-ray and 14.4 keV γ ray spectra in backscattering geometry [*Klingelhöfer et al.*, 2003]. Spirit did so for all targets until sol 461, when the instrument was commanded to collect only 14.4 keV spectra. Opportunity has collected 6.4 keV and 14.4 keV spectra for all targets to date. The Fe mineralogy of rock and soil targets at Gusev Crater and Meridiani Planum reported by *Morris et al.* [2004, 2006a, 2006b, also Iron mineralogy and aqueous alteration in the Columbia Hills of Gusev crater from Husband Hill through Home Plate by the Mars Exploration Rover Mössbauer Spectrometer, submitted to *Journal of Geophysical Research*, 2007], *Klingelhöfer et al.* [2004] and D. Rodionov et al. (manuscript in preparation, 2008) has been exclusively extracted from 14.4 keV spectra. The focus of this paper is the analysis and Monte Carlo simulation of 6.4 keV and 14.4 keV MER Mössbauer spectra of Adirondack Class rocks from Gusev crater and laboratory spectra of layered samples obtained with a MER-equivalent instrument.

[3] The evaluation of MER Mössbauer data is described by *Morris et al.* [2006a]. Briefly, MIMOS II measures spectra in 13 temperature windows [*Klingelhöfer et al.*, 2003]. For the analyses presented in this paper, all available temperature windows for a specific target have been

[1]Institut für Anorganische und Analytische Chemie, Johannes Gutenberg-Universität, Mainz, Germany.
[2]NASA Johnson Space Center, Houston, Texas, USA.
[3]Space Research Institute IKI, Moscow, Russia.
[4]Department of Physics, University of Guelph, Guelph, Ontario, Canada.
[5]Vallourec Research Center, Aulnoye-Aymeries, France.
[6]Now at Tasmanian ICT Centre, CSIRO, Hobart, Tasmania, Australia.

0148-0227/08/2007JE003022$09.00

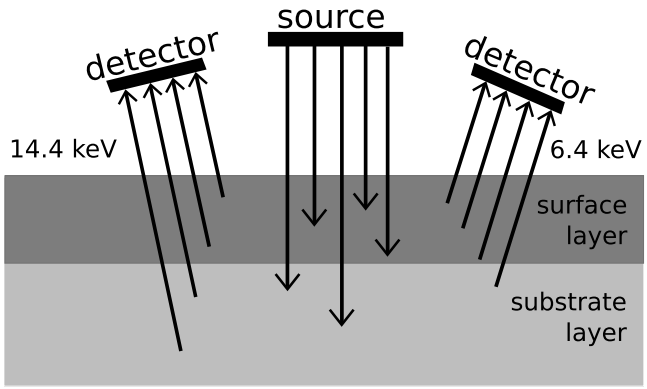

Figure 1. Illustration of depth selectivity: a two-layer sample is irradiated by a Mössbauer source. A resonant absorption of 14.4 keV γ rays is followed by either the emission of 14.4 keV γ rays or 6.4 keV X rays. A 6.4 keV spectrum bears more information about the near-surface part of a sample.

summed to improve counting statistics. An in-house fitting routine was used. The Mössbauer parameters isomer shift (δ), quadrupole splitting (ΔE_Q), and the magnetic hyperfine field strength (B_{hf}, only for sextet subspectra) were constrained to the values reported by *Morris et al.* [2006a] for all 14.4 keV and 6.4 keV spectra. All subspectra were fit using Lorentzian line shapes. The identification of minerals is not the focus of this paper and was adopted from *Morris et al.* [2006a].

[4] The analysis of both 6.4 keV and 14.4 keV Mössbauer spectra provides depth selective information about the mineralogical composition of Fe-bearing phases, because photon penetration depths are energy-dependent. The backscattering MB spectra derived from the less energetic 6.4 keV X rays stem from shallower depths and contain more information about the near-surface part of a sample than do the more energetic 14.4 keV γ rays as shown schematically in Figure 1. Therefore, spectra obtained on samples with a thin surface layer such as a weathering rind will show significant differences in their 6.4 keV and 14.4 keV spectra.

[5] In order to understand and quantify the effect of surface layers of various thickness and composition on MER Mössbauer spectra, we (1) obtained equivalent measurements on laboratory samples composed of a mineral thin section or metallic iron foil on top of a thick substrate material with a MER-equivalent Mössbauer spectrometer and (2) modeled the scattering of Mössbauer radiation using Monte Carlo simulations. The simulations allow the independent variation of parameters such as the thickness, mineralogical composition, and density of a layered sample. The comparison of measured spectra obtained on layered laboratory samples with calculated spectra serves to validate the Monte Carlo code. The thickness of surface layers such as weathering rinds can then be estimated by comparison to Monte Carlo simulated spectra.

[6] Comparison of 6.4 keV and 14.4 keV spectra for Adirondack Class rocks shows that the derived subspectral areas are different. An apparent enrichment of Fe from olivine in 6.4 keV spectra compared to 14.4 keV, is observed. In order to understand the origin of this difference, which is not related to a detectable surface layer and is probably a general result and not just restricted to Adirondack Class rocks, we obtained laboratory and Monte Carlo spectra for two terrestrial olivine basalt samples.

2. Depth Selectivity in Mössbauer Spectra

[7] Mössbauer spectroscopy of Fe-bearing samples requires a nuclear source of 14.4 keV γ rays (typically ^{57}Co embedded in a Rh metal matrix). These γ rays are absorbed resonantly by ^{57}Fe nuclei in the sample (2.2% natural abundance). The ^{57}Co decay to ^{57}Fe occurs with 91% probability via the 14.4 keV excited state of ^{57}Fe. In the further decay to the ground state, a 14.4 keV γ ray is emitted with 9% probability. The remaining 91% are accounted for by the emission of X rays and electrons, following internal conversion processes. The Fe-Kα line at 6.4 keV occurs in $\sim$75% of all photon deexcitation events, which makes it viable for Mössbauer spectroscopy. The electrons emitted during the decay include conversion electrons with energies up to 14.3 keV as well as Auger- and shake-off-electrons with energies in the range of less than 15 eV up to several keV. The decay of ^{57}Co is illustrated in Figure 2; the characteristics of the ^{57}Co decay are discussed in detail by *Browne et al.* [1986].

[8] Mössbauer spectra separately obtained for resonant γ rays, X rays, and conversion electrons for a homogenous, thick Fe-bearing target should all be the same because they all "sample" the same Fe-bearing material. Conversely, Mössbauer spectra obtained for the same radiations can be different if the target is heterogeneous with respect to Fe-bearing phases because the different radiations have different scale lengths for absorption. For example, the penetration (or escape) depth for the resonant electrons, X rays, and γ rays increases in the same order.

[9] Therefore, information about the distribution of Fe-bearing phases with depth (depth sensitive or selective), is possible if two or more resonant radiations are measured for the same sample. Depth-sensitive information is possible for the MER MIMOS II instruments because both the resonant 14.4 keV γ rays and the resonant 6.4 keV X rays are simultaneously detected [*Klingelhöfer et al.*, 2002, 2003; *de Souza*, 2004; *Fleischer*, 2006; *Fleischer et al.*, 2007]. Analysis of 14.4 keV and 6.4 keV backscatter Mössbauer spectra is discussed by *Bara* [1980] and *Mei et al.* [1988].

[10] The maximum sampling depth of the Mössbauer 14.4 keV γ rays is on the order of $\sim$500 μm in coherent rock of basaltic composition, while 6.4 keV X rays have a maximum sampling depth of $\sim$200 μm (section 5 of this paper; see also *Morris et al.* [2000]). Conversion electron Mössbauer spectroscopy (CEMS) makes use of conversion electrons with energies of up to 14.3 keV, resulting in sensitivity to the first $\sim$0.2 μm of a sample [*Salvat and Parellada*, 1984; *Gellert et al.*, 1993]. A possible application of CEMS is the investigation of very thin iron films as described by *Tyliszczak et al.* [1983].

[11] Low-energy electron Mössbauer spectroscopy (LEEMS) utilizes Auger- and shake-off-electrons with energies of <15 eV. These low-energy electrons constitute

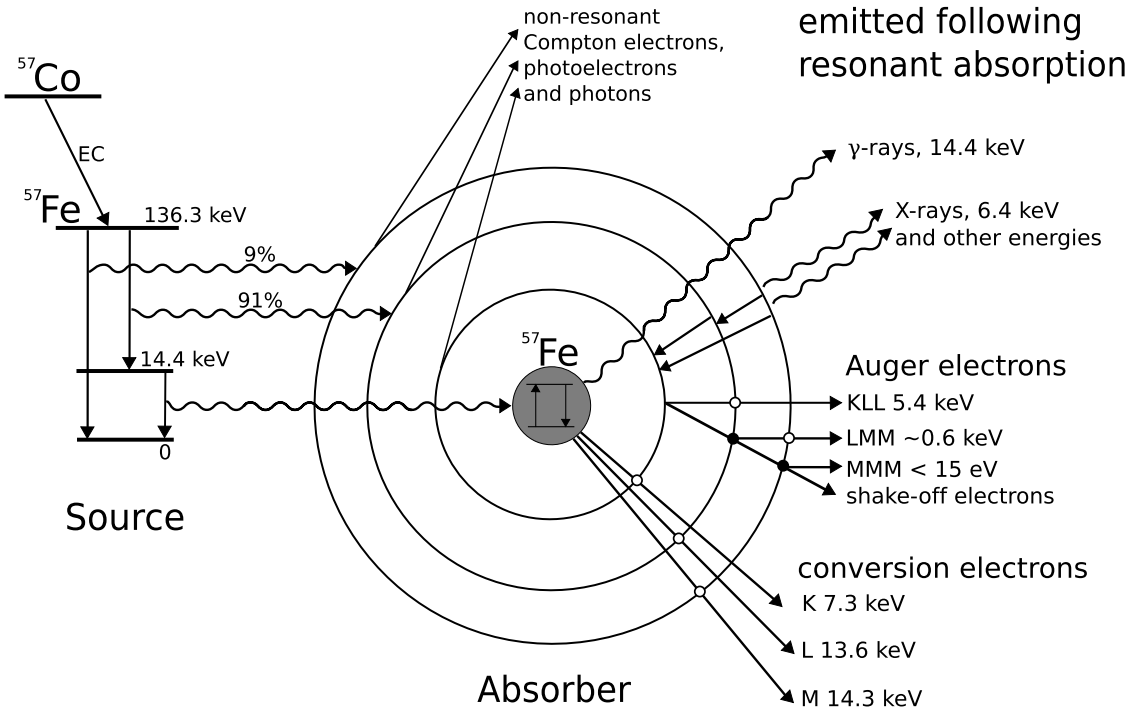

Figure 2. Overview of emission processes of photons and electrons during the decay of ^{57}Co to ^{57}Fe and deexcitation of ^{57}Fe (modified from *de Grave et al.* [2005]).

more than 50% of the integral CEMS signal [*Zabinski and Tatarchuk*, 1988; *Klingelhöfer and Kankeleit*, 1990] and lead to a sampling depth of ~0.005 μm [*Vandenberghe et al.*, 1998; *Klingelhöfer and Kankeleit*, 1990; *Klingelhöfer et al.*, 1992; *de Grave et al.*, 2005]. A possible application of ILEEMS is the investigation of the phase composition of Fe oxide surfaces as described by *de Grave et al.* [2005]. We are currently building an ILEEMS (integral LEEMS) setup to supplement the depth selectivity reached by MIMOS II [*Hahn*, 2007].

3. Absorption and Reemission Processes

[12] The mathematical description of photon interaction processes in a sample forms the basis of a Monte Carlo simulation and will be described in this section. Generally, all photons can interact through the photoelectric effect, Compton and Rayleigh scattering and pair production [e.g., *Siegbahn*, 1968]. Pair production occurs for energies from a threshold of 1.022 MeV and can therefore be neglected for photons produced in the decay of ^{57}Co, which have energies up to 706.4 keV [*Kistner and Sunyar*, 1965]. In the case of ^{57}Fe Mössbauer spectroscopy, 14.4 keV γ quanta can be absorbed resonantly.

[13] In the energy range below 14.4 keV, the nonresonant process which occurs with the highest probability by far is the photoelectric effect. Photons with higher energies (especially 122.2 keV and 136.3 keV) occur in the decay of ^{57}Co and contribute to the background of the spectrum through scattering processes. The intensity $I(x)$ of a γ ray at a certain depth x in a sample is given by

$$I(x) = I_0 e^{-\mu x}, \tag{1}$$

where I_0 is the incident intensity. The absorption coefficient μ can be calculated from atomic cross sections σ_i for the different photon interaction processes i:

$$\mu = \frac{N_A}{A}\rho \sum_i \sigma_i w_i, \tag{2}$$

where N_A is the Avogadro constant, A is the atomic mass number, ρ is the density of the sample, and w_i represents the weight percentages of different elements. The total absorption cross section is composed of the cross sections for the different processes:

$$\sigma_{total} = \sigma_{resonant} + \sigma_{photo} + \sigma_{Compton} + \sigma_{Rayleigh}. \tag{3}$$

[14] The absorption cross section for resonant absorption is determined by [e.g., *Wegener*, 1966]

$$\sigma_{res}(E_\gamma) = f\beta\sigma_0 \frac{\Gamma^2}{4} \sum_i \left(\frac{1}{(E_\gamma - E_{res,i})^2 + \frac{\Gamma^2}{4}} \right), \tag{4}$$

where β is the isotopic fraction of ^{57}Fe (2.2%), σ_0 is the maximum resonant cross section, Γ is the natural line width of the source, E_γ is the energy of the emitted photon and E_{res} the energy at resonance. The probability for recoilless emission and absorption of γ rays is given by the f factor, which is often referred to as the Debye-Waller factor (and sometimes as the Lamb-Mössbauer factor). Generally, Fe^{2+} ions have smaller f factors than Fe^{3+} ions. We applied an f factor correction to subspectral areas determined from fits to account for this difference using an average value of

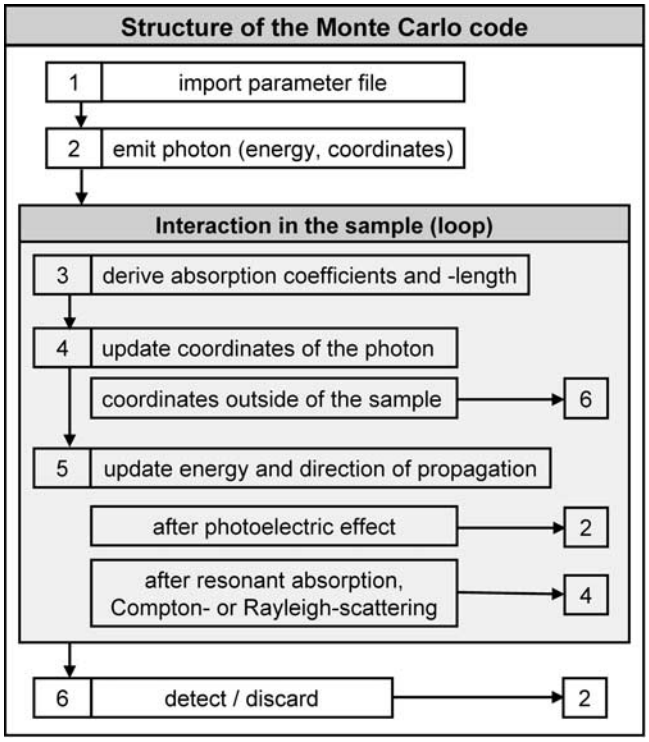

Figure 3. The structure of the Monte Carlo code. It models the backscattering geometry of the MIMOS II setup and a sample composed of two distinct, homogeneous layers. The emission, interaction processes, and detection of photons are simulated for one photon after another.

f(Fe3+)/f(Fe2+) = 1.21 [*de Grave and Van Alboom*, 1991; *Morris et al.*, 1995].

[15] The cross sections for photoelectric absorption (σ_{photo}) and for Compton and Rayleigh scattering ($\sigma_{C,R}$) on an atom with atomic number Z are given by [e.g., *Grupen*, 1993]:

$$\sigma_{photo}(E_\gamma) = \left(\frac{32}{\varepsilon^7}\right)^{1/2} \alpha^4 Z^5 \frac{8}{3}\pi r_e^2,\ \varepsilon = \frac{E_\gamma}{m_e c^2}. \tag{5}$$

$$\sigma_{C,R}(E_\gamma) = 2Z\pi r_e^2 \left\{ \left(\frac{1+\varepsilon}{\varepsilon}\right)\left[\frac{2(1+\varepsilon)}{1+2\varepsilon} - \frac{1}{\varepsilon}\ln(1+2\varepsilon)\right] + \frac{1}{2\varepsilon}\ln(1+2\varepsilon) - \frac{1+3\varepsilon}{(1+2\varepsilon)^2} \right\}. \tag{6}$$

In equations (5) and (6), m_e is the electron mass, r_e is the classical electron radius, and α is the fine structure constant.

[16] After an interaction through either Compton or Rayleigh scattering, the angle θ between the incident and scattered direction of propagation of the photon is determined according to the forward-backward-symmetric Thomson distribution [e.g., *Kleinknecht*, 1992]:

$$T(\theta) = 1 + \cos^2\theta. \tag{7}$$

Rayleigh scattering does not effect the energy of a photon. The energy of a Compton-scattered photon is determined by [e.g., *Kleinknecht*, 1992]

$$E'_\gamma = \frac{E_\gamma}{1 + \varepsilon(1 - \cos\theta_\gamma)}, \tag{8}$$

where θ_γ is the scattering angle of the photon.

4. Monte Carlo Simulations

[17] Mössbauer spectra of layered samples are influenced by various parameters, such as the thickness of the layers, the density of the sample, and its elemental composition, especially, the iron content. A Monte Carlo simulation allows for the independent variation of these parameters to study their influence on 6.4 keV and 14.4 keV spectra. The comparison of simulated and measured spectra can then be used to estimate the thickness of a surface layer. A detailed description of the Monte Carlo simulation developed for the work presented in this paper is given by *Fleischer* [2006]. The simulation models the geometry of the MIMOS II instrument [*Klingelhöfer et al.*, 2003]. A sample composed of two distinct, homogeneous layers, each containing up to ten different Mössbauer subspectra (singlets, doublets, and sextets) can be modeled.

[18] The Monte Carlo code is based on the equations discussed in section 2. The structure of the code is illustrated in Figure 3. At the start of the program, a parameter file is imported, which contains values defining the geometry and physical properties of the sample and the Mössbauer parameters and line widths for each subspectrum. For every photon, its emission from the Mössbauer source, interaction processes in the sample, and detection are simulated, updating its energy and direction of propagation after each interaction. The simulated Mössbauer source emits photons with an energy of 14.4 keV, which is then modified according to the source velocity. After a resonant absorption at a certain depth in the sample, both 14.4 keV γ rays and 6.4 keV X rays can be emitted, but as the absorption and scattering processes in the sample have energy-dependent probabilities, only 14.4 keV γ rays reach the detectors from greater depths. A real Mössbauer source emits photons with energies above and below 14.4 keV. Photons with higher energy (especially 122.2 keV and 136.3 keV) contribute to the constant background level of both spectra, photons with lower energy contribute to the constant background level of the 6.4 keV spectrum. The interactions of such photons do not depend on the source velocity. They don't affect the structure of a Mössbauer spectrum, merely reduce its statistical quality. Thus, these photons are not modeled to reduce the number of photons necessary for a spectrum of good signal-to-noise-ratio and thereby the runtime of a simulation.

[19] In the sample, all photons can interact nonresonantly through Compton and Rayleigh scattering as well as the photoelectric effect. Only 14.4 keV γ rays can be absorbed resonantly through the Mössbauer effect. The probabilities for these four processes are determined by absorption coefficients. In the simulation, equation (4) is used to calculate absorption coefficients for resonant absorption.

Table 1. Elemental composition, densities, and Mössbauer parameters δ, ΔE_Q, and B_{hf} at 298 K for Substrates and Surface Layers Used for Laboratory Measurements on Layered Samples[a]

	Physical Properties		MB Parameters[b]		
Sample	Composition (wt %)	Density, (g/cm^3)	δ (mm/s)	ΔE_Q (mm/s)	B_{hf} (T)
Olivine thin section,[c] 60 μm	44% O, 19%Si, 6% Fe, 31% Mg	3.1 ± 0.6	1.15	3.00	-
Metallic Fe foils	100% Fe	7.5 ± 1.1	0	0	33.0
Pyrite substrate[d]	47% Fe, 53% S	4.9 ± 0.1	0.32	0.62	-
Hematite substrate[d]	70% Fe, 30% O	5.5 ± 0.9	0.37	−0.19	51.6

[a]Elemental composition is derived from EDX measurements, Mössbauer parameters are δ, the isomer shift relative to metallic Fe foil; ΔE_Q the quadrupole splitting; and B_{hf}, the hyperfine field.
[b]The uncertainty in δ and ΔE_Q is 0.02 mm/s, the uncertainty in B_{hf} is 0.8 T.
[c]Olivine from Twin Sisters Range, Washington.
[d]Unknown origin.

Instead of the natural source line width defined in equation (4), the ''minimum observable width'' (twice the natural line width) is used [*Muir et al.*, 1966].

[20] Absorption coefficients for nonresonant interaction processes and their dependence on the elemental composition and the photon energy are taken from the ''X-Com'' tables (described by M. J. Berger et al. (X-COM: Photon cross sections database, 2005, available at http://physics.nist.gov/PhysRefData/Xcom/html/xcom1.html)). This approach is more convenient than calculating absorption coefficients using equations (2), (5), and (6). Each interaction process may alter the energy and direction of propagation of a photon. After the resonant absorption of a 14.4 keV γ ray, the absorbing Fe nucleus reaches an excited state. In its decay back to the ground state, 14.4 keV γ rays as well as X rays and electrons are emitted. The emission of a 6.4 keV X ray is five times more likely than the reemission of a 14.4 keV γ ray. Emissions of photons with energies between 6 keV and 14.4 keV are modeled according to the decay characteristics of the ^{57}Fe excited state [*Browne et al.*, 1986]. Photons with energies as low as 6 keV contribute to the spectra because of finite detector resolution (the detector resolution at room temperature is ~1.0–1.5 keV [*Klingelhöfer et al.*, 2003]). Emissions of photons with energies below 6 keV are neglected, because they do not contribute to the spectra. The reemission of electrons, including conversion electrons, following resonant absorption, may lead to velocity-correlated 6.4 keV X rays. The contribution of these electrons to the spectra is currently not included in the simulation. The reemission after a resonant absorption is modeled with an isotropic distribution. Compton scattering alters the energy of a photon according to equation (8). Rayleigh scattering does not alter the energy. In both cases, the scattering occurs according to the forward-backward symmetric Thomson distribution given by equation (7). The photoelectric effect is modeled as the complete absorption of a photon. In the simulation, the photon is discarded, and the next run starts by generating a new photon from the Mössbauer source.

[21] The modeling of a photon's detection takes into account its energy and coordinates. If a photon's direction of propagation crosses the detectors, and if its energy lies within the assumed detector resolution of 1 keV, the photon is detected. X rays with energies of ~6.4 keV are accumulated in one spectrum, γ rays with energies of ~14.4 keV in a second spectrum. The energy channels of each spectrum are defined by the Doppler velocity of the source at the time of the photon's emission. The detectors have an efficiency of nearly 100% at 6.4 keV and ~70% at 14.4 keV [*Klingelhöfer et al.*, 2003]. To minimize the runtime of a simulation, the detectors are modeled as having an efficiency of 100% for both energies.

[22] The two spectra are exported as separate data files which can then be fitted using the same fitting routine that is also used to fit measured spectra. This approach allows for a direct comparison of measured and simulated spectra. A total number on the order of 10^8 photons is required to obtain simulated spectra of good quality.

5. Layered Samples: Laboratory Measurements and Simulations

[23] In order to investigate the depth selectivity in Mössbauer spectra experimentally, samples composed of two distinct, homogeneous layers of well known composition were analyzed using a laboratory version of MIMOS II instruments employed by the MER rovers [*Klingelhöfer et al.*, 2003]. An olivine thin section with a thickness of 60 μm or iron foils with thicknesses of 10 and 50 μm, respectively, were combined with substrates of pyrite (FeS_2)

Table 2. Subspectral Areas of Substrate From Measured and Simulated Spectra of Layered Samples[a]

Sample		14.4 keV		6.4 keV	
Surface Layer	Substrate	Measured,[b] %	Simulated, %	Measured, %	Simulated,%
Olivine (60 μm)[c]	Pyrite	67	63	37	36
Fe foil (10 μm)[d]	Pyrite	17	17	13	8
Olivine (60 μm)	Hematite	77	74	53	54
Fe foil (50 μm)	Hematite	2	2	1	1

[a]Subspectral areas are not *f* factor corrected; substrate is pyrite or hematite.
[b]The uncertainty in subspectral areas is ±2% absolute.
[c]The uncertainty in thickness is ±10 μm.
[d]The uncertainty in thicknesses of Fe foils is ±15%.

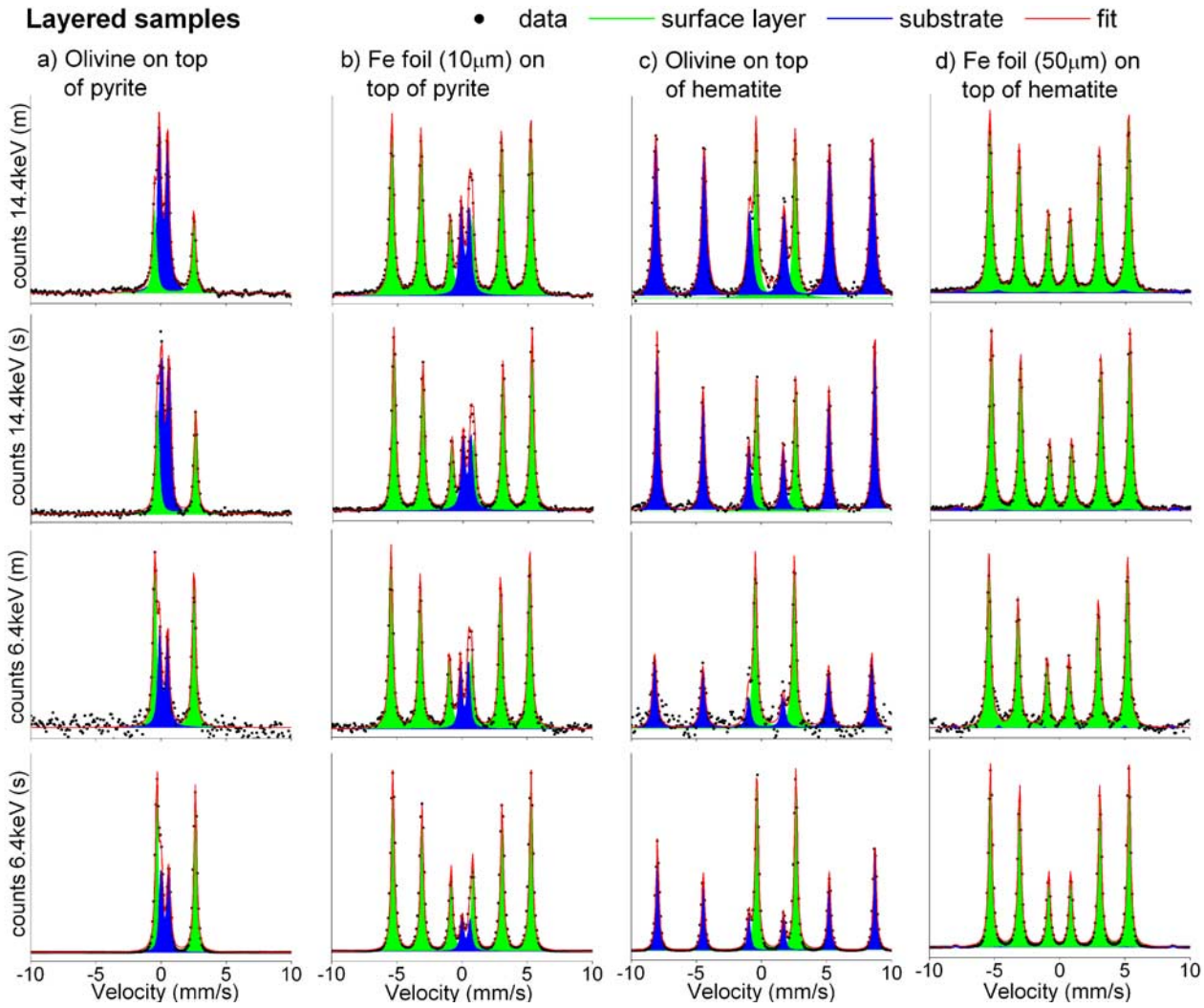

Figure 4. Measured spectra obtained on layered laboratory samples and the corresponding simulated spectra, from top to bottom: 14.4 keV measured (m); 14.4 keV simulated (s); 6.4 keV measured (m); and 6.4 keV simulated (s). All measurements were performed at room temperature. Zero velocity is referenced with respect to metallic iron foil. Mössbauer areas derived from the spectra shown here are given in Table 2.

and hematite (α-Fe_2O_3). These samples were chosen because they differ significantly in their iron content, and their different hyperfine parameters render them easy to distinguish in spectra. Table 1 gives a summary of elemental composition, derived from Energy Dispersive X-Ray (EDX) Analysis, and Mössbauer parameters. The Mössbauer parameters determined from component subspectra that are relevant for phase identification are the isomer shift (δ) and quadrupole splitting (ΔE_Q) for doublet subspectra, and δ, ΔE_Q and the magnetic hyperfine field strength (B_{hf}) for sextet subspectra. All laboratory measurements were conducted at room temperature.

[24] MB spectra were obtained for four target configurations (Table 2). Iron foils were used for technical reasons: Iron foils can be manufactured with a homogeneous thickness and it is convenient to use durable foils instead of brittle thin sections with high iron content (e.g., hematite). Furthermore, iron foils, having a well-defined thicknesses and being composed of just one element, are also easy to simulate. In contrast to most other elements, the iron absorption coefficients for 6.4 keV and 14.4 keV photons are very similar due to the iron K edge at 7.1 keV. Thus, measurements with an iron surface layer lead to similar subspectral areas of the substrate layer in both spectra.

[25] Spectra obtained on these samples illustrate the range of relative Mössbauer areas caused by layers of varying thickness and iron content. The results obtained from these well-defined samples proved to be helpful for the understanding of spectra obtained on natural samples of varying composition with surface layers such as coatings or weathering rinds with varying thicknesses.

[26] Figure 4 compares measured and the corresponding simulated spectra obtained on these layered samples in both 6.4 keV and 14.4 keV. Mössbauer subspectral areas obtained from measured (calculated from least squares fit of the spectra) and simulated spectra are summarized in Table 2.

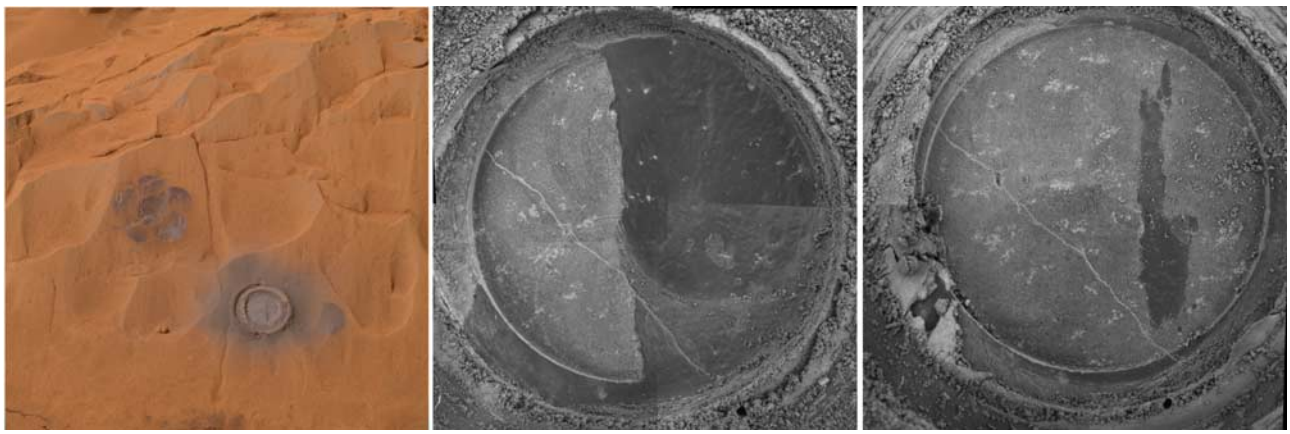

Figure 5. (left) Pancam image (P2530 sequence) with a brush pattern and an abraded depression after the second RAT grind (http://marswatch.astro.cornell.edu/pancam_instrument/images/True/Sol087A_P2530_1_True_RAD.jpg). (middle) MI mosaic obtained after the first grind showing a dark coating (courtesy NASA/JPL-Caltech, PIA05658). (right) MI mosaic obtained after the second grind showing a remnant of the dark coating (courtesy NASA/JPL-Caltech, PIA05661). Both MI mosaics measure ~45 mm across.

Values are given as a percentage of the total area. The values given in Table 2 are not *f* factor corrected.

[27] In Figure 4, it is also apparent that the simulated 14.4 keV spectra are noisier than the simulated 6.4 keV spectra, contrary to measured spectra. This is a consequence of the model used for the ^{57}Co source in the simulation, as described in section 4: this simulated source emits only 14.4 keV γ rays. Thus, the large number of 6.4 keV X rays emitted from a real ^{57}Co source contributing only to the constant background level of a measured 6.4 keV spectrum is absent in simulated 6.4 keV spectra.

[28] In general, Mössbauer areas obtained from measured and simulated spectra agreed within ~5% (absolute). With a 50 μm thick iron foil as the surface layer, the hematite substrate with an iron content of ~70 wt % shows a subspectral area of 1% in the 6.4 keV and ~3% in the 14.4 keV spectrum, which is close to the detection limit. A 50 μm thick Fe layer can therefore be regarded as the maximum thickness which allows the substrate to be resolved in Mössbauer spectra. The γ ray intensity after passing through this layer can be derived from equation (1), using absorption coefficients for 14.4-keV γ rays from the X-Com tables. Taking into account the backscattering geometry of the experiment (i.e., the surface layer is passed twice before the radiation reaches the detectors), the calculated intensity is 0.78% for 14.4 keV γ rays and 0.60% for 6.4 keV X rays. These values can be used to estimate the maximum thickness of surface layers with other compositions. We estimated the maximum thicknesses of two different surface layers that are necessary to allow detection of the substrate at the detection limit. For a surface layer composed of hematite (Fe_2O_3) with a density of 5.3 g/cm^3, we calculated a thickness of ~100 μm for 14.4 keV γ rays, and ~90 μm for 6.4 keV X rays. For a surface layer having 20% FeO and 80% SiO_2 and a density of 3 g/cm^3, which is a simplification of typical Martian samples [e.g., *Gellert et al.*, 2004], we calculated a maximum depth of ~530 μm for 14.4 keV γ rays, and ~130 μm for 6.4 keV X rays.

[29] These values are consistent with earlier results [*Morris et al.*, 2000; *Klingelhöfer et al.*, 2003], where the maximum depth of a surface layer is defined to absorb 95% of the incident radiation, taking into account attenuation processes on the way in and out of the sample, that is, passing the surface layer twice. With this approach, *Morris et al.* [2000] calculate a maximum depth of ~200 μm for a basaltic composition.

[30] Differences between measured and simulated spectra will always arise because it is not possible to model the exact composition and geometry of the sample. Impurities and inhomogeneities can be modeled in principle, but are not taken into account in the current model, which assumes two homogeneous layers. The surface layer is modeled with a constant thickness, which is an obvious simplification of reality. In addition, broadening of the line widths resulting from temperature effects or impurities in the crystal structure, is not modeled in the Monte Carlo code at present. As a consequence, line widths tend to be narrower in simulated spectra, even though measured line widths are used as an input for the simulations.

[31] The results presented in this section show that the Fe mineralogical composition of a surface layer and its substrate can be determined by comparing 6.4 keV and 14.4 keV Mössbauer spectra if the surface layer is not too thick. With the help of a Monte Carlo simulation, it is possible to estimate the thickness of a surface layer such as a weathering rind.

6. Application to Mars

[32] During the first 100 sols of its mission at Gusev crater, the ''Spirit'' rover investigated 5 basaltic rocks (Adirondack, Humphrey, Paperback, Mazatzal, and Route66), which on the basis of their chemical composition were grouped as Adirondack class rocks [*McSween et al.*, 2006; *Ming et al.*, 2006; *Morris et al.*, 2006a; *Squyres et al.*, 2006]. Mössbauer spectra were obtained on the undisturbed surfaces of all rocks, on the brushed surfaces of all rocks

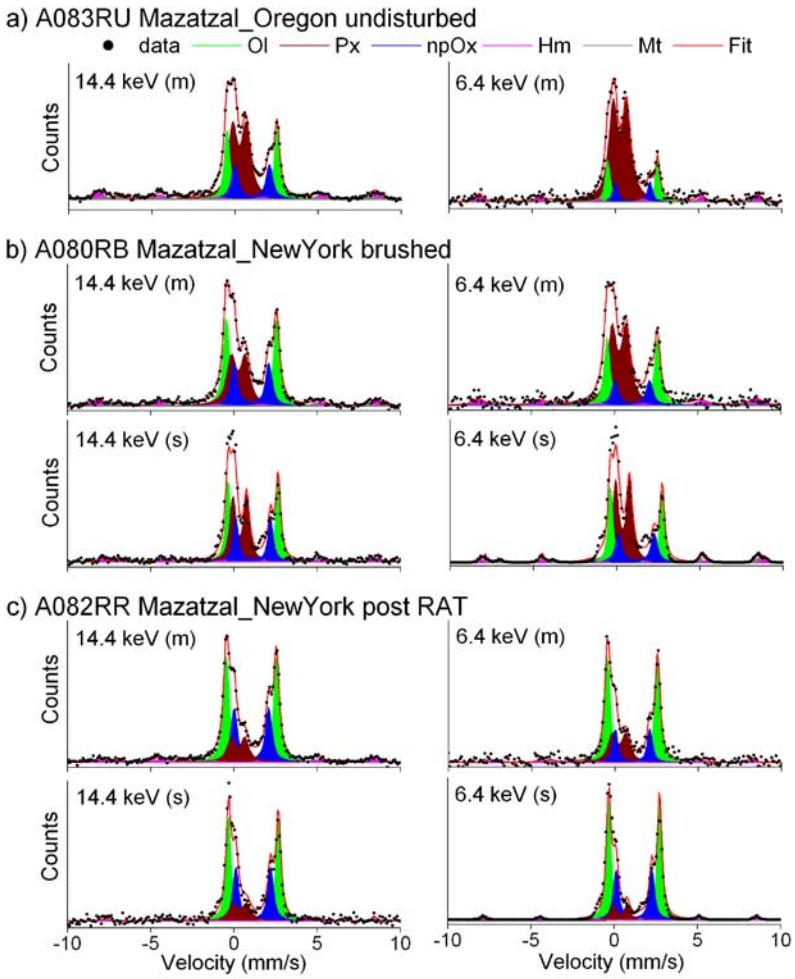

Figure 6. Measured spectra obtained on the rock "Mazatzal" and the corresponding simulated spectra (m, measured; s, simulated). Measured spectra from all available temperature windows (200–250 K) were summed. Spectra obtained (a) on the undisturbed surface of the rock; (b) on the brushed rock surface; and (c) after the second RAT grind. Zero velocity is referenced with respect to metallic iron foil. Mössbauer areas derived from the spectra shown here are given in Table 3. Ol, olivine; Px, pyroxene; npOx, nanophase ferric oxide; Hm, hematite; Mt, magnetite.

except Paperback, and after grinding with the RAT on Adirondack, Humphrey, and Mazatzal. The spectra reveal a basaltic mineralogical composition with only minor alteration with respect to Fe-bearing phases. On average, 51% of total iron in the Mössbauer spectra is from olivine, 34% from pyroxene, 8% from magnetite, 6% from nanophase ferric oxide (npOx) and 1% from hematite [*Morris et al.*, 2006a].

6.1. Mazatzal Coatings

[33] Figure 5 shows Pancam images and MI mosaics of the rock Mazatzal. A dark surface layer was detected on this rock with the MI after the first of two RAT grinding operations. This surface layer was removed except for a remnant in a second grind. Measured and simulated Mazatzal spectra are shown in Figure 6. The Martian spectra were obtained on the undisturbed dusty surface of the target "Oregon" and on the target "New York" after brushing and after the second RAT grind. In comparison with 14.4 keV spectra, 6.4 keV spectra obtained on the undisturbed and brushed surface clearly show an enrichment of npOx (Figures 6a and 6b), which is not the case for spectra obtained after the second RAT grind (Figure 6c). The subspectral area of npOx decreases considerably from pregrind to postgrind spectra, while the subspectral areas of olivine and pyroxene increase. These results demonstrate that the surface layer on Mazatzal is enriched in npOx as compared to the bulk composition of the rock. The ratio of the subspectral areas of olivine and pyroxene remains stable in all measurements, which is consistent with the assumption that the surface layer is composed of mainly npOx with regard to iron-bearing minerals [*Schröder*, 2006]. APXS data show an enrichment of S and Cl in the surface layer [*Gellert et al.*, 2004]. The dark layer was interpreted to result from aqueous alteration, the source of increased Fe^{3+} being mainly oxidation of olivine and pyroxene [*Haskin et al.*, 2005; *Hurowitz et al.*, 2006].

[34] Spectra obtained on the brushed and abraded surface of Mazatzal were compared to simulated spectra to estimate the thickness of the dark alteration layer. Spectra obtained

Table 3. Subspectral Areas Derived From Measured Spectra Obtained on Adirondack Class Rocks and Simulated Mazatzal Spectra for Both 6.4 keV and 14.4 keV[a]

Sample	Spectrum	Ol (%)	Px (%)	npOx (%)	Hm (%)	Mt (%)
A018RU Adirondack_Blue	14.4 keV (m)	48[b]	30	7	4	12
	6.4 keV (m)	59	19	9	3	9
A033RB Adirondack_Blue	14.4 keV (m)	46	34	7	1	12
	6.4 keV (m)	59	22	8	1	11
A034RR Adirondack_Blue	14.4 keV (m)	52	25	7	2	14
	6.4 keV (m)	68	15	8	2	7
A058RU Humphrey_AshleyJ	14.4 keV (m)	43	34	8	4	11
	6.4 keV (m)	56	24	8	6	5
A059RB Humphrey_Heyworth1	14.4 keV (m)	44	31	9	4	11
	6.4 keV (m)	57	22	9	5	8
A060RR Humphrey_Heyworth2	14.4 keV (m)	51	30	6	3	10
	6.4 keV (m)	70	18	7	3	3
A076RU Paperback_Appendix	14.4 keV (m)	45	31	20	0	3
	6.4 keV (m)	53	14	29	0	4
A079RU Mazatzal_NewYork	14.4 keV (m)	36	25	29	5	5
	6.4 keV (m)	29	13	47	11	0
A080RB Mazatzal_NewYork	14.4 keV (m)	41	21	29	5	4
	14.4 keV (s)	40	23	29	5	3
	6.4 keV (m)	34	11	47	5	2
	6.4 keV (s)	32	19	39	6	4
A082RR Mazatzal_NewYork	14.4 keV (m)	51	28	13	3	6
	14.4 keV (s)	53	31	12	3	1
	6.4 keV (m)	58	17	19	0	7
	6.4 keV (s)	61	29	8	3	0
A083RU Mazatzal_Oregon	14.4 keV (m)	29	18	40	7	6
	6.4 keV (m)	18	9	62	9	2
A084RR Mazatzal_Brooklyn	14.4 keV (m)	58	30	6	1	5
	6.4 keV (m)	71	18	5	0	5
A094RU Route66_Candidate7	14.4 keV (m)	50	35	11	0	4
	6.4 keV (m)	49	28	9	0	14
A100RB Route66_SoHo	14.4 keV (m)	56	35	7	0	2
	6.4 keV (m)	74	18	8	0	0

[a]Spectra are (m) measured and (s) simulated Mazatzal. Target naming convention (adopted from *Morris et al.* [2006a]) is Awwwxy Feature-name_Target-name: A is MER-A; www is sol number (data returned to Earth); xy is target type (RU, rock undisturbed; RB, rock brushed; RR, rock RAT-ground). Ol, olivine; Px, pyroxene; npOx, nanophase ferric oxides; Hm, hematite; Mt, magnetite. Values are given as percentage of total area and are f factor corrected.

[b]Uncertainty in subspectral areas is ±2% absolute.

on the undisturbed surface have not been included in the simulations, as simulating these spectra would require a three-layer model (dust, alteration rind, and substrate). Mössbauer areas for all Adirondack class rocks determined from measured and simulated spectra are given in Table 3. The Mössbauer parameters for 14.4 keV spectra for all samples (Tables 4a and 4b) are reported by *Morris et al.* [2006a]. For the simulations, a simple model of the mineralogical composition was used. This model is given in Table 5. It takes into account the normative CIPW calculations presented by *McSween et al.* [2006], which use subspectral areas and Fe^{3+}/Fe_T derived from Mössbauer spectra and chemistry from APXS data. For APXS measurements of the Fe concentration, 50% of the intensity of X rays originates from a depth of 22.5 μm [*Rieder et al.*, 2003]. Measurements on Mazatzal show a slight increase in iron content from pregrind to postgrind measurements (16.7% FeO, target Oregon, undisturbed surface; 18.0%, target New York, postgrind) [*Gellert et al.*, 2004]. Thus, the surface layer and the substrate seem to have very similar iron contents.

[35] Nonresonant absorption processes occur in non-Fe-bearing minerals. To account for these minerals, the model employs SiO_2 as a substitute, which facilitates calculation of absorption coefficients because of its simple chemical composition. This approach is applicable for three reasons: First, the absorption coefficients of SiO_2 are in the same order of magnitude as those of other non-Fe-bearing silicates or oxides. Second, SiO_2 is a likely remnant of olivine weathering processes: the removal of iron from olivine ($(Fe,Mg)SiO_4$) leaves behind a combination of Mg and SiO_2. Third, not accounting for Fe-absent minerals would yield unphysically high iron contents. The composition given in Table 5 in combination with a thickness of 10 μm of the surface layer yields the best agreement between measurements and simulations. For simulations of postgrind spectra, the surface layer thickness is assumed equal to zero. The remaining differences between measured and simulated spectra, especially in the case of 6.4 keV spectra, are presumably resulting from the rather simple model used in the simulation.

[36] One obvious difference between measured and simulated spectra is the occurrence of two peaks in simulated spectra (at ~ -1 and +2 mm/s). These are at the positions of the central peaks of the magnetic phases hematite and magnetite. The intensity ratios of these peaks are modeled based on measured intensity ratios. We are investigating why their signature is stronger in simulated spectra.

[37] With $\sim$23 wt % Fe in the substrate and $\sim$18 wt % in the surface layer, the model slightly overestimates the iron

Table 4a. Mössbauer Parameters δ and ΔE_Q for Olivine, Pyroxene, and npOx in Adirondack Class Rocks as Reported by *Morris et al.* [2006a][a]

	Olivine		Pyroxene		npOx	
Sample	δ(mm/s)	ΔE_Q (mm/s)	δ (mm/s)	ΔE_Q (mm/s)	δ (mm/s)	ΔE_Q (mm/s)
A018RU Adirondack_Blue	1.15[b]	3.00[b]	1.15	2.07	0.40	0.87
A033RB Adirondack_Blue	1.16	2.96	1.16	2.04	0.41	0.84
A034RR Adirondack_Blue	1.15	2.94	1.15	2.04	0.38	0.79
A058RU Humphrey_AshleyJ	1.16	3.01	1.15	2.11	0.38	0.75
A059RB Humphrey_Heyworth1	1.16	3.00	1.16	2.10	0.38	0.75
A060RR Humphrey_Heyworth2	1.16	3.02	1.16	2.07	0.35	0.79
A076RU Paperback_Appendix	1.15	2.97	1.16	2.03	0.36	0.88
A079RU Mazatzal_NewYork	1.16	3.03	1.17	2.10	0.37	0.84
A080RB Mazatzal_NewYork	1.16	3.02	1.16	2.08	0.37	0.83
A082RR Mazatzal_NewYork	1.16	3.01	1.16	2.07	0.35	0.82
A083RU Mazatzal_Oregon	1.14	3.00	1.14	2.08	0.37	0.80
A084RR Mazatzal_Brooklyn	1.15	2.98	1.14	2.05	0.36	0.85
A094RU Route66_Candidate7	1.16	3.01	1.16	2.08	0.38	0.99
A100RB Route66_SoHo	1.16	3.01	1.16	2.08	0.38	0.99

[a]These parameters were used to fit both 14.4 keV and 6.4 keV spectra.
[b]Uncertainty is ±0.02 mm/s.

content in comparison with APXS data. However, it yields the correct mineral fractions, which is of more importance for Mössbauer spectra than the overall iron content. Modeling a thinner layer of 5 μm yields too much olivine and pyroxene, even with a pure npOx composition. With a model of thicker surface layers (up to 30 μm), no composition can be found which yields an acceptable agreement between simulation and measurement simultaneously for 6.4 keV and 14.4 keV spectra.

6.2. Differences in 6.4 keV and 14.4 keV Spectra Obtained on Homogeneous Samples

[38] Differences between 6.4 keV and 14.4 keV spectra cannot always be attributed to the existence of a surface layer. As long as no surface layer is present, approximately the same subspectral areas (within statistical errors) would ideally be expected in 6.4 keV and 14.4 keV spectra. Contrary to this expectation, subspectral areas show deviations in most measurements.

[39] For a detailed analysis, Mössbauer areas obtained from 6.4 keV and 14.4 keV spectra of Adirondack class rocks (Table 3) were plotted against each other for olivine, pyroxene, nanophase ferric oxide (npOx), hematite and magnetite (Figure 7). Measurements with the same areas in 6.4 keV and 14.4 keV spectra should plot on a line through the origin with slope 1. The two dashed blue lines indicate a region of less than 5% deviation (absolute) between both spectra. Different rocks are indicated by a particular color. Measurements on undisturbed surfaces, after brushing and after RAT grinding are indicated by squares, circles, and triangles, respectively.

[40] An apparent enrichment of olivine, in combination with an apparent depletion of pyroxene, in the 6.4 keV spectra is evident for most of the measurements (Figures 7a and 7b). Exceptions are spectra obtained on the undisturbed or brushed surface of Mazatzal, which show a depletion of olivine in 6.4 keV spectra in correlation with an enrichment of npOx (Figure 7c). These differences can be attributed to the surface layer on Mazatzal. Nanophase ferric oxide does not show large differences between 6.4 and 14.4 keV spectra obtained on other Adirondack class rocks. No obvious trend can be found in the plots for hematite and magnetite in spectra of Adirondack class rocks resulting from their comparably low concentration and thus low signal-to-noise ratio (Figures 7d and 7e). The differences between Mössbauer areas in 6.4 keV and 14.4 keV spectra in Figures 7a–7c cannot be explained by statistical errors. The relative area of olivine is slightly increasing from pregrind to postgrind measurements in both 6.4 keV and 14.4 keV spectra (see Table 3).

[41] In principle, the higher olivine intensity in 6.4 keV spectra can be explained with the existence of an olivine-enriched surface layer. However, olivine is one of the least stable minerals toward aqueous weathering and should therefore be depleted relative to pyroxene in a surface layer exposed to aqueous weathering. For mechanical weathering,

Table 4b. Mössbauer Parameters δ, ΔE_Q, and B_{hf} for Hematite and Magnetite in Adirondack Class Rocks as Reported by *Morris et al.* [2006a][a]

	δ (mm/s)	ΔE_Q (mm/s)	B_{hf} (T)
All hematite-bearing samples	0.37	−0.16	51.7
All magnetite-bearing samples tet-Fe^{3+}	0.31	0.06	50.1
All magnetite-bearing samples oct-$Fe^{2.5+}$	0.64	0.00	46.9

[a]These parameters were used to fit both 14.4 keV and 6.4 keV spectra. The uncertainty in δ and ΔE_Q is 0.02 mm/s, the uncertainty in B_{hf} is 0.8 T.

Table 5. Composition of the Surface Layer and Unweathered Interior of Mazatzal Used for Monte Carlo Simulations

		Concentration (wt %)	
Fe-Bearing Mineral	Composition (wt %)	Rind	Interior
Olivine	50% Fe_2SiO_4 + 50% Mg_2SiO_4	15	45
Pyroxene	33% $CaFeSi_2O_6$ + 33% $CaMgSi_2O_6$ + 33% $MgFeSi_2O_6$	15	35
npOx	20% Fe_2O_3 + 80%SiO_2[a]	60	10
Hematite	50% Fe_2O_3 + 50%SiO_2	10	0
Magnetite	50% Fe_3O_4 +50% SiO_2	0	10
Total		100	100

[a]SiO_2 is used as a substitute for all minerals not containing iron.

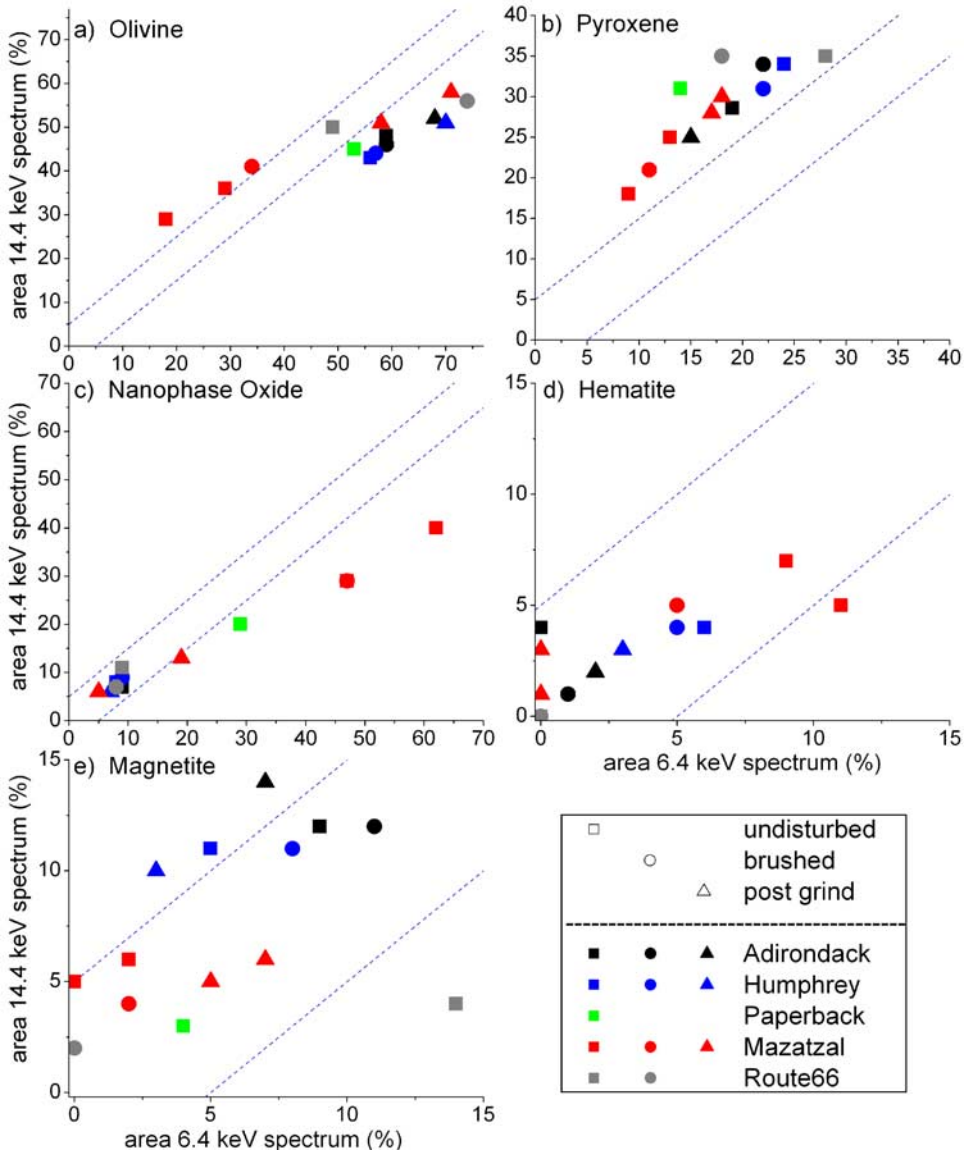

Figure 7. Comparison of relative Mössbauer areas obtained from 6.4 and 14.4 keV spectra of Adirondack class rocks. For the minerals (a) olivine, (b) pyroxene, (c) npOx, (d) hematite, and (e) magnetite, the relative areas from 14.4 keV spectra are plotted against the relative areas from 6.4 keV spectra. The dashed blue lines each represent a difference of 5% (absolute) between both spectra. The upper line is equivalent to a 5% larger area in 14.4 keV spectra; the lower line is equivalent to a 5% larger area in 6.4 keV spectra.

a possible explanation is given by *Rasmussen et al.* [2005]: Mechanical weathering or grinding may remove whole pyroxene crystals, while the weaker olivine crystals simply break up and largely remain on the surface. This results in a surface region with a higher olivine/pyroxene ratio than the rock as a whole, thus leading to an enhanced olivine intensity in 6.4 keV spectra compared to 14.4 keV spectra.

[42] To find explanations for the observed deviations, we compared spectra obtained on Mars to laboratory samples and simulations. *McSween et al.* [2006] describe olivine clasts in Adirondack class rocks. To investigate the influence of olivine clasts in a basaltic matrix on 6.4 keV and 14.4 keV Mössbauer spectra experimentally, a sample of terrestrial olivine basalt was obtained from the quarry Bauersberg, Rhoen, Germany. This sample contains olivine crystals up to ~5 mm in diameter in a pyroxene-rich matrix. A second basalt sample containing both olivine and pyroxene crystals with diameters of less than ~2 mm was measured for comparison. This sample was obtained from Ortenberg, Vogelsberg, Germany. On both samples, freshly exposed natural surfaces were measured.

[43] Figure 8a compares 6.4 keV and 14.4 keV spectra obtained on the abraded surface of the rock Humphrey, showing an apparent enrichment of olivine (or depletion of pyroxene) in the 6.4 keV spectrum compared to the 14.4 keV spectrum. The subspectral area of olivine is 70% in the 6.4 keV spectrum and 51% in the 14.4 keV spectrum. Similar observations were made for the other

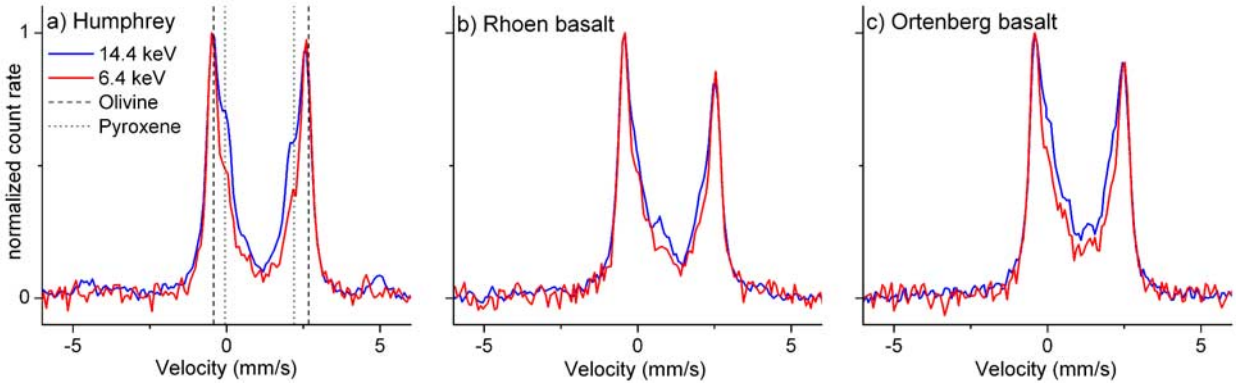

Figure 8. (a) Measured spectra obtained on the rock Humphrey, 14.4 keV and 6.4 keV in direct comparison, show an apparent enrichment of olivine in the 6.4 keV spectrum. (b) and (c) Measured spectra obtained on two terrestrial olivine basalts. For better comparison, all spectra are normalized to equal olivine intensities.

Adirondack class rocks. Figure 8b shows measured spectra obtained on the Rhoen basalt sample. The relative Mössbauer areas of olivine are 60% in the 6.4 keV spectrum, along with 23% pyroxene and 17% npOx, and 54% in the 14.4 keV spectrum along with 28% pyroxene and 18% npOx. Figure 8c shows spectra obtained on the Ortenberg basalt. The relative Mössbauer areas of olivine are 51% in the 6.4 keV spectrum, along with 39% pyroxene and 10% ilmenite, and 38% in the 14.4 keV spectrum along with 50% pyroxene and 12% ilmenite. The pyroxene area is composed of three subspectra (see *Fegley et al.* [1995] for comparison). Thus, all three rock samples show more olivine in the 6.4 keV spectrum compared to the 14.4 keV spectrum. The effect is less pronounced in the Rhoen basalt sample and also less pronounced in spectra obtained on powdered Ortenberg basalt (44% olivine, 42% pyroxene and 14% ilmenite in the 6.4 keV spectrum compared to 41% olivine, 45% pyroxene and 15% ilmenite in the 14.4 keV spectrum). We are currently investigating further reasons for an enhancement of olivine in 6.4 keV spectra, such as influences of sample crystallinity, crystal zoning and chemical composition.

[44] Mössbauer spectra of hypothetical rocks containing variable proportions of olivine and pyroxene were Monte Carlo simulated for comparison. The models for both minerals were adopted from the simulations of Mazatzal spectra described in section 6.1, with compositions as given in Table 5. A mixture of 60 wt% olivine and 40 wt % pyroxene yields subspectral areas of olivine of 67% in the 6.4 keV spectrum and 62% in the 14.4 keV spectrum. A mixture of 40 wt % olivine and 60 wt % pyroxene yields subspectral areas of olivine of 35% in the 6.4 keV spectrum and 32% in the 14.4 keV spectrum. Thus, simulated 6.4 keV spectra show larger olivine areas than simulated 14.4 keV spectra. Subspectral areas may be influenced by different line widths in 6.4 and 14.4 keV spectra. Thus, a physically reasonable model of line widths has to be implemented in the Monte Carlo code to determine whether the observations stem from real effects or whether they are an artifact in simulated spectra. Line widths in 6.4 and 14.4 keV spectra are discussed in section 7.

[45] Modeling these spectra accurately is challenging. Crystals in a matrix cannot be simulated at present, because the Monte Carlo code models a homogeneous sample. More work is needed to understand and subsequently model the influence of a sample's composition, crystallinity and porosity on line widths in Mössbauer spectra. Additionally, temperature and thickness effects have to be taken into account.

7. Line Widths in 6.4 keV and 14.4 keV Spectra

[46] When comparing measured and simulated 6.4 keV and 14.4 keV spectra, attention must be paid to differences in line widths. As discussed in section 5, line widths in measured spectra are influenced by sample composition and crystallinity as well as temperature and thickness effects. Thickness effects have a greater influence on line widths in 14.4 keV spectra, which can additionally broaden because of self absorption [e.g., *Gütlich et al.*, 1978; *Mitra*, 1992, and references therein]. As a result, line widths tend to be broader in 14.4 keV spectra than in 6.4 keV spectra. These effects are not included in the simulation, which imports constant line widths from a parameter file. Varying line widths in simulations has a slight effect on subspectral areas, leading to small deviations (less than 5% absolute) between 6.4 keV and 14.4 keV spectra. To improve the comparability of measured and simulated spectra, a physically reasonable simulation of line widths is important. This can be accomplished by first analyzing line widths experimentally.

[47] We investigated the line widths in 6.4 keV and 14.4 keV spectra obtained on Adirondack class rock spectra for the two minerals with the largest subspectral areas, olivine and pyroxene. The result is illustrated in Figures 9a and 9b. The two axes represent the line widths from both spectra, so that a measurement with the same line widths in 6.4 keV and 14.4 keV spectra would plot on a line through origin with slope 1 (dashed blue line). For 14.4 keV spectra, Figures 9a and 9b show that pyroxene line widths are generally broader than olivine line widths. This is the expected result because the M1 and M2 sites in pyroxene are more different than in olivine [e.g., *Mitra*, 1992]. For

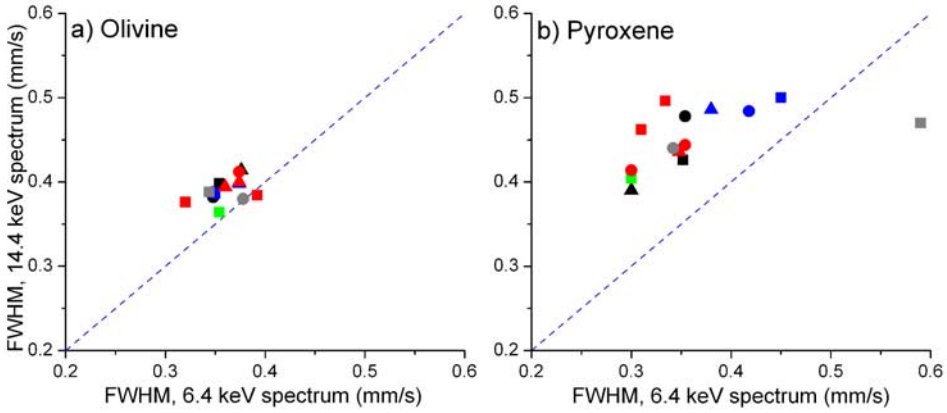

Figure 9. Mössbauer line widths (FWHM) obtained from spectra of Adirondack class rocks; 14.4 keV versus 6.4 keV for the minerals (a) olivine and (b) pyroxene. Identical line widths in both spectra are represented by the dashed line. See Figure 8 for legend.

6.4 keV spectra, pyroxene and olivine line widths lie in the same range. In the comparison of 6.4 and 14.4 keV spectra, olivine line widths are rather similar (Figure 9a), while pyroxene line widths are generally broader in 14.4 keV spectra (Figure 9b). Pyroxenes may exhibit zoning with respect to Fe concentrations [e.g., *Stolper and McSween*, 1979]. Because of the greater sampling depth of 14.4 keV γ rays, a larger compositional variation may be sampled, leading to larger line widths in 14.4 keV spectra. Further investigations are needed to understand the origin of these differences.

8. Summary and Conclusions

[48] 1. A Monte Carlo code was developed to simulate Mössbauer spectra obtained with 6.4 keV X rays and 14.4 keV γ rays. The code can be used to estimate the thickness of thin surface layers that have different Fe-mineralogical compositions than the substrate.

[49] 2. The Monte Carlo code was validated against 6.4 keV and 14.4 keV backscatter Mössbauer spectra of layered samples whose Fe-mineralogical composition and surface layer thickness were known.

[50] 3. On the basis of measured and Monte Carlo simulated and 6.4 keV and 14.4 keV spectra obtained on the rock Mazatzal at Gusev crater, a thickness of $\sim$10 μm was estimated for the thickness of its dark surface layer (weathering rind).

[51] 4. Adirondack class rocks show an apparent enrichment of olivine in 6.4 keV spectra compared to 14.4 keV spectra. An enrichment of olivine in 6.4 keV spectra compared to 14.4 keV spectra also occurs in spectra obtained on terrestrial olivine basalt samples. This effect can also be observed in Monte Carlo simulated spectra of a mixture of olivine and pyroxene, but is close to the limit of precision for areas.

[52] Additional laboratory and modeling investigations are needed to understand this difference between 6.4 keV and 14.4 keV Mössbauer spectra, including additional sample analysis and implementation of models for dust layers and inhomogeneities in the Monte Carlo code.

[53] **Acknowledgments.** Development of the MIMOS II Mössbauer spectrometer was funded by the German Space Agency under contract 50QM99022 and supported by the Technical University of Darmstadt and the University of Mainz. The support of the Russian space agency is acknowledged. C.S. acknowledges support by an appointment to the NASA Postdoctoral Program at the Johnson Space Center, administered by Oak Ridge Associated Universities through a contract with NASA. We acknowledge the unwavering support of JPL engineering and MER operations staff and the MER Athena Science Team. We thank E. de Grave for permission to reproduce Figure 2. This paper benefited from the comments of an anonymous reviewer and from a very thorough review by David Agresti.

References

Bara, J. J. (1980), Analysis of Mössbauer scattering spectra, *Phys. Status Solidi A*, *58*(2), 349–359, doi:10.1002/pssa.2210580204.

Browne, E., R. B. Firestone, and V. S. Shirley (1986), *Table of Radioactive Isotopes*, John Wiley, New York.

de Grave, E., and A. Van Alboom (1991), Evaluation of ferrous and ferric Mössbauer fractions, *Phys. Chem. Miner.*, *18*, 337–342.

de Grave, E., R. E. Vandenberghe, and C. Dauwe (2005), ILEEMS: Methodology and applications to iron oxides, *Hyperfine Interact.*, *161*, 147–160, doi:10.1007/s10751-005-9177-1.

de Souza, P. A. (2004), Extraterrestrial and terrestrial outdoor applications of Mössbauer spectroscopy, Ph.D. thesis, Johannes-Gutenberg-Univ. Mainz, Mainz, Germany.

Fegley, B., G. Klingelhöfer, R. A. Brackett, N. Izenberg, D. T. Kremser, and K. Lodders (1995), Basalt oxidation and the formation of hematite on the surface of Venus, *Icarus*, *118*, 373–383, doi:10.1006/icar.1995.1197.

Fleischer, I. (2006), Quantifizierung der Tiefenselektivität von 14,4-keV- und 6,4-keV-Strahlung in Mössbauer-Spektren, Diploma thesis, Johannes-Gutenberg-Univ. Mainz, Mainz, Germany.

Fleischer, I., et al. (2007), Weathering rinds on Gusev Crater rocks: Simulation of 6.4-keV and 14.4-keV backscatter Mössbauer spectra and implications on depth selectivity, *Lunar Planet. Sci.*, *XXXVIII*, Abstract 1701.

Gellert, R., et al. (1993), Depth selective CEMS in the energy range 0 to 20 keV, *Nucl. Instrum. Methods Phys. Res., Sect. B*, *76*, 381–382, doi:10.1016/0168-583X(93)95246-2.

Gellert, R., et al. (2004), Chemistry of rocks and soils in Gusev Crater from the Alpha Particle X-ray Spectrometer, *Science*, *305*, 829–832, doi:10.1126/science.1099913.

Grupen, C. (1993), *Teilchendetektoren*, B I Wissenschaftsverlag, Bibliogr. Inst., Mannheim, Germany.

Gütlich, P., et al. (1978), *Mössbauer Spectroscopy and Transition Metal Chemistry*, Springer, Berlin, Germany.

Hahn, M. (2007), Aufbau eines Hochvakuum Konversionselektronen-Mössbauerspektrometers zur Untersuchung von eisenhaltigen Proben mit ILEEMS, Diploma thesis, Johannes-Gutenberg-Univ. Mainz, Mainz, Germany.

Haskin, L., et al. (2005), Water alteration of rocks and soils on Mars at the Spirit rover site in Gusev Crater, *Nature*, *436*, 66, doi:10.1038/nature03640.

Hurowitz, J. A., S. M. McLennan, N. J. Tosca, R. E. Arvidson, J. R. Michalski, D. W. Ming, C. Schröder, and S. W. Squyres (2006), In situ and experimental evidence for acidic weathering of rocks and soils on Mars, *J. Geophys. Res.*, *111*, E02S19, doi:10.1029/2005JE002515.

Kistner, O. C., and A. W. Sunyar (1965), Excited states of Fe^{57} populated in Co^{57} decay, *Phys. Rev.*, *139*, B295–B299, doi:10.1103/PhysRev.139.B295.

Kleinknecht, K. (1992), *Detektoren für Teilchenstrahlung*, Teubner Studienbücher, Stuttgart, Germany.

Klingelhöfer, G., and E. Kankeleit (1990), Conversion electron Mössbauer spectroscopy with very low energy (0 to 15 eV) electrons, *Hyperfine Interact.*, *57*, 1905–1910, doi:10.1007/BF02405740.

Klingelhöfer, G., U. Imkeller, E. Kankeleit, and B. Stahl (1992), Remarks on depth selective CEMS–backscattering measurements, *Hyperfine Interact.*, *71*, 1445–1448, doi:10.1007/BF02397355.

Klingelhöfer, G., et al. (2002), The Miniaturized Mössbauer Spectrometer MIMOS II for extraterrestrial and outdoor terrestrial applications: A status report, *Hyperfine Interact.*, *144–145*, 371–379, doi:10.1023/A:1025444209059.

Klingelhöfer, G., et al. (2003), Athena MIMOS II Mössbauer spectrometer investigation, *J. Geophys. Res.*, *108*(E12), 8067, doi:10.1029/2003JE002138.

Klingelhöfer, G., et al. (2004), Jarosite and hematite at Meridiani Planum from Opportunity's Mössbauer Spectrometer, *Science*, *306*, 1740–1745, doi:10.1126/science.1104653.

McSween, H. Y., et al. (2006), Characterization and petrologic interpretation of olivine-rich basalts at Gusev Crater, Mars, *J. Geophys. Res.*, *111*, E02S10, doi:10.1029/2005JE002477.

Mei, Z., B. Fultz, and J. W. Morris (1988), Intensities of backscatter Mössbauer spectra, *J. Appl. Phys.*, *64*(5), 2550–2555.

Ming, D. W., et al. (2006), Geochemical and mineralogical indicators for aqueous processes in the Columbia Hills of Gusev crater, Mars, *J. Geophys. Res.*, *111*, E02S12, doi:10.1029/2005JE002560.

Mitra, S. (1992), *Applied Mössbauer Spectroscopy*, Pergamon, Oxford, U.K.

Morris, R. V., D. C. Golden, J. F. Bell III, and H. V. Lauer Jr. (1995), Hematite, pyroxene, and phyllosilicates on Mars: Implications from oxidized impact melt rocks from Manicouagan Crater, Quebec, Canada, *J. Geophys. Res.*, *100*(E3), 5319–5328, doi:10.1029/94JE01500.

Morris, R. V., et al. (2000), Mineralogy, composition, and alteration of Mars Pathfinder rocks and soils: Evidence from multispectral, elemental, and magnetic data on terrestrial analogue, SNC meteorites, and Pathfinder samples, *J. Geophys. Res.*, *105*(E1), 1757–1817, doi:10.1029/1999JE001059.

Morris, R. V., et al. (2004), Mineralogy at Gusev Crater from the Mössbauer Spectrometer on the Spirit Rover, *Science*, *305*, 833–836, doi:10.1126/science.1100020.

Morris, R. V., et al. (2006a), Mössbauer mineralogy of rock, soil, and dust at Gusev Crater, Mars: Spirit's journey through weakly altered olivine basalt on the plains and pervasively altered basalt in the Columbia Hills, *J. Geophys. Res.*, *111*, E02S13, doi:10.1029/2005JE002584.

Morris, R. V., et al. (2006b), Mössbauer mineralogy of rock, soil, and dust at Meridiani Planum, Mars: Opportunity's journey across sulfate-rich outcrop, basaltic sand and dust, and hematite lag deposits, *J. Geophys. Res.*, *111*, E12S15, doi:10.1029/2006JE002791.

Muir, A. H., K. J. Ando, and H. M. Coogan (1966), *Mössbauer Effect Data Index 1958–1965*, Wiley-Interscience, New York.

Rasmussen, H., et al. (2005), Magnetic properties of Martian olivine basalt studied by terrestrial analogues, *Hyperfine Interact.*, *166*, 561–566, doi:10.1007/s10751-006-9341-2.

Rieder, R., et al. (2003), The new Athena alpha particle X-ray spectrometer for the Mars Exploration Rovers, *J. Geophys. Res.*, *108*(E12), 8066, doi:10.1029/2003JE002150.

Salvat, F., and J. Parellada (1984), Theory of conversion electron Mössbauer spectroscopy (CEMS), *Nucl. Instrum. Methods Phys. Res., Sect. B*, *1*, 70–84, doi:10.1016/0168-583X(84)90481-6.

Schröder, C. (2006), Weathering of Fe-bearing minerals under extraterrestrial conditions, investigated by Mössbauer spectroscopy, Ph.D. thesis, Johannes Gutenberg-Univ. Mainz, Mainz, Germany.

Siegbahn, K. (1968), *Alpha-, Beta-, and Gamma-Ray Spectroscopy*, North-Holland, Amsterdam, Netherlands.

Squyres, S. W., et al. (2004), The Spirit Rover's Athena Science Investigation at Gusev Crater, Mars, *Science*, *305*, 794–799, doi:10.1126/science.3050794.

Squyres, S. W., et al. (2006), Rocks of the Columbia Hills, *J. Geophys. Res.*, *111*, E02S11, doi:10.1029/2005JE002562.

Stolper, E., and H. Y. McSween Jr. (1979), Petrology and origin of the shergottite meteorites, *Geochim. Cosmochim. Acta*, *43*, 1475–1498, doi:10.1016/0016-7037(79)90142-X.

Tyliszczak, T., J. A. Sawicki, and W. Wilk (1983), Conversion electron Mössbauer spectroscopy of very thin iron films: Ultra-high vacuum equipment and preliminary measurements, *Hyperfine Intact.*, *16*, 1001–1004, doi:10.1007/BF02147406.

Vandenberghe, R. E., E. de Grave, E. van San, M. A. Ahmed, and C. Dauwe (1998), Integrated low energy electron Mössbauer spectroscopy (ILEEMS), *Phys. Mag.*, *20*(4), 339–353.

Wegener, H. (1966), *Der Mössbauer-Effekt und seine Anwendungen in Physik und Chemie*, Bibliogr. Inst., Mannheim, Germany.

Zabinski, J. S., and B. J. Tatarchuk (1988), Resonant low energy electrons and their impact on sampling depth during backscatter-electron Mössbauer spectroscopy, *Nucl. Instrum. Methods Phys. Res., Sect. B*, *31*, 576–583, doi:10.1016/0168-583X(88)90458-2.

P. A. de Souza, Tasmanian ICT Centre, CSIRO, Castray Esplanade, Hobart, Tas 7000, Australia.

I. Fleischer, M. Hahn, and G. Klingelhöfer, Institut für Anorganische und Analytische Chemie, Johannes Gutenberg-Universität, D-55128 Mainz, Germany. (fleischi@uni-mainz.de)

R. Gellert, Department of Physics, University of Guelph, MacNaughton Building, Gordon Street, Guelph, ON, N1G 2W1, Canada.

R. V. Morris and C. Schröder, NASA Johnson Space Center, Astromaterials Research and Exploration Science Mail Code KR, 2101 NASA Parkway, Houston, TX 77058, USA.

D. Rodionov, Space Research Institute IKI, 117997, 84/32 Profsoyuznaya Street, Moscow, Russia.